

# A Novel Approach to Facile Synthesis and Biosensing of the Protein-Regulated Graphene

*Esfandyar Askari, Seyed Morteza Naghib\**

Nanotechnology Department, School of New Technologies, Iran University of Science and Technology (IUST), P.O. Box 16846 – 13114, Tehran, Iran

\*E-mail: [naghib@iust.ac.ir](mailto:naghib@iust.ac.ir)

*Received: 21 September 2017 / Accepted: 16 November 2017 / Published: 16 December 2017*

---

In this study, we synthesized graphene through a green approach in which consuming of the chemical materials in production process decreased and reached to the lowest value. Bovine Serum Albumin (BSA) was used as the stabilizer for exfoliated graphene sheets. Synthesis of the functionalized graphene was confirmed by uv-vis spectroscopy. The physical and chemical properties of the synthesized graphene were compared with conventional graphene oxide. Atomic force microscopy (AFM) was utilized to the evaluating the thickness of graphene sheets. Functional groups of graphene were determined by FTIR spectroscopy and Raman spectra supported the AFM and FTIR results. Main electrochemical properties of the graphene were studied by cyclic voltammetry (CV) and electrochemical impedance spectroscopy (EIS). In the following, a biosensing application was investigated to determine ascorbic acid (AA) via a non-enzymatic interaction between the graphene and AA. The present graphene-modified BSA (G-BSA) based sensor provided a favorable opportunity for the design of non-enzymatic electrochemical sensors with extraordinary performance via higher some sensing characteristics and simple fabrication.

---

**Keywords:** graphene, bovine serum albumin, electrochemistry, biosensing applications

## 1. INTRODUCTION

Nanoparticles have opened a wide range of applications in the fields of energy system, industry, and biomedicine due to exhibiting extraordinary and unique physicochemical characteristics such as electrical, thermal, and mechanical properties [1, 2]. The newest graphitic nanomaterials, graphene, have gained a great deal of interesting in the scientific community due to their novel and amazing characteristics and wide range of potential applications [2, 3]. According to IUPAC definition, graphene is a single carbon layer of graphite structure, in which a two-dimensional honeycomb lattice was arranged by sp<sup>2</sup> bonded carbon atoms [3, 4].

Since graphene was discovered in 2004, many applications were established in nanoscience and nanotechnology [3]. In the electrochemical research area, carbon electrodes have a lot of applications

due to its wide anodic potential range, low residual current, availability, chemical inertness, and reduced cost [5]. Excellent features such as good mechanical rigidity, negligible porosity and other good properties endow suitable position to carbon based materials in the electroanalytical sensors. Carbon nanotube (CNT) possess good stability and sensitivity respect to another carbon based materials, but the characteristic role of the metal impurities in the electrochemical activity and the graphitic edge present in CNT were has been challenges that limited their applications [5, 6]. According to the nature of graphene structure, the electrons have linear dispersion relation, and act as massless relativities species that are suitable for electronic fields. The electrons move ballistically in graphene layer without scattering with mobility exceeding  $15000 \text{ m}^2\text{v}^{-1}\text{s}^{-1}$  at room temperature [2].

Alwarappan, et al compared the electrochemical properties of SWCNT and graphene and found that graphene is stable, possess better signal-to-noise ratio, sensitivity and conductivity. In other hand, the high surface negative charge density of graphene in comparison with SWCNT is an important feature in the sensor applications [5, 7]. For regulating the electronic properties of graphene, many efforts were carried out but the side effects of these nanostructures alter the intrinsic structure of graphene and biocompatibility [8-13]. Sharma and coworkers increased the sensitivity of graphene immunosensor by the use of the graphene contained oxygen functional group that caused fast electron transfer [14]. Actually, functionalization of graphene with polymers [15], immobilization of biomolecules on the surface of graphene [16] and decoration with positively charged nanoparticles [17] are such methods that improved graphene based electrochemical sensors.

Many methods have been reported for synthesis of graphene, but some applications of graphene have limited its synthesis method. Moreover, the additional experimental steps and exogenous materials have created toxicity challenges in the use of graphene [4]. Synthesis of graphene via exfoliating the graphite in water media is a suitable method for production of aqueous graphene dispersion in biomedical application and overcome the challenges [4].

In this study, we synthesized green graphene through a facile and low cost method. In this approach, graphite in the presence of protein solution was exfoliated. Bovine serum albumin (BSA) is a natural protein, in which there are polar and nonpolar amino acids in its structure. These amino acids are capable to stabling the exfoliated graphene in the aqueous solution [18, 19]. To verification of the synthesized graphene, spectroscopic techniques were applied. Then graphene was qualified with AFM, Raman spectroscopy and scanning electron microscopy (SEM). As well as, the electrochemical properties of graphene were evaluated. Finally, the functionalized graphene was applied to determine ascorbic acid (AA) as a non-enzymatic biosensor.

## **2. EXPERIMENTAL**

### *2.1. Materials and synthesis*

#### *2.1.1. Reagents and solvents*

Graphite powder,  $\text{KMnO}_4$ ,  $\text{H}_2\text{SO}_4$ ,  $\text{H}_2\text{O}_2$ , bovine serum albumin an HCL were purchased from Merck. Dialysis membrane was obtained from Sigma-Aldrich. All chemicals and solvents were used without further purification.

### 2.1.2. Synthesis of G-BSA

50 mg BSA powder was mixed with 1 L of Deionized water at  $\sim 30^{\circ}\text{C}$  for  $\sim 14$  h. The pH of the aqueous BSA solution was adjusted to  $\sim 3.6$  with HCl. Then, 1 g of graphite was added to the solution and mixed for 30 min with magnitude stirrer. The mixture was transferred to the probe ultra-sonication system and sonicated for 5 hours. The power of sonicated solution was fixed to 9W. After that, solution was kept for 20 days for sedimentation of the large graphene and unexfoliated graphite. The sediment of mixture was removed and the solution was centrifuged at 4000 rpm for 20 min. Finally, the supernatant was collected and dried [18, 19]. The schematic representation of the synthesis procedure was illustrated in Fig. 1.

### 2.1.3. Synthesis of graphene oxide (GO)

Graphene oxide was synthesized via modified hummer method. In the absence of  $\text{NaNO}_3$ , oxidation of natural graphite was performed in the reaction system.

First, graphite powder (3 g) was added to the concentrated  $\text{H}_2\text{SO}_4$  (70 ml) and stirred in ice bath. Under forcefully stirring,  $\text{KMnO}_4$  (9 g) was slowly added and kept at the temperature under  $20^{\circ}\text{C}$ . Then, solution was transferred to a  $40^{\circ}\text{C}$  oil bath and vigorously stirred for 30 min. In the following, 150 mL deionized water was added and stirred at  $95^{\circ}\text{C}$  for 15 min. In the next step, 500 mL deionized water and then  $\text{H}_2\text{O}_2$  (15 mL) was slowly added. The dark brown color of solution was turned to yellow G-BSA show oxidation step were established. The solution was washed and filtered with 1:10 HCl (250 mL) to remove metal ions. Residual solids were dried in the air and diluted with 600 mL of  $\text{H}_2\text{O}_2$ . The dialysis membrane with a molecular cut off of 8000-14000 g/mole was applied for removing the remaining metal spices. The resultant graphite oxide aqueous dispersion was diluted in 1.5 L deionized water and stirred for 24 h. For exfoliating graphite oxide, solution was sonicated for 30 min. the GO dispersion was then centrifuged with 3000rpm for 40 min to remove unexfoliated graphite oxide [20, 21].

## 2.2. Characterization

### 2.2.1 Spectroscopic analysis

Ultraviolet-visible (uv-vis) absorption spectra of G-BSA and GO were measured with T80+UV/VIS spectrometer Instruments Ltd. where the light path length was 1cm. FTIR spectra of samples were recorded on IR spectrometer (8500S SHIMADZU) at frequencies ranging 400 to 4000  $\text{cm}^{-1}$ . Raman spectra were recorded over 500-400  $\text{cm}^{-1}$  with an excitation wavelength of 642 nm using RFS-100/S Raman spectrophotometer equipment.

### 2.2.2. Study of surface morphology

Atomic Force Microscopy (AFM) images of samples were measured using a scanning probe microscope (veeco, USA). SEM images were obtained on a (TE-SCAN) field emission scanning electron microscopy.

2.2.3. Electrochemical analysis

All electrochemical measurements were investigated by the use of a Potentiostat/Galvanostat model Autolab PGSTAT 30 (Echo chemie, B. V.) by Nova 1.11 software. The electrochemical impedance spectroscopy (EIS) studies were performed within the frequency range of 10-1–105 Hz, with the potential amplitude of 14 mV around the open circuit potential ( $E_{ocp}=0.22$  V).

3. RESULTS AND DISCUSSION

3.1. Uv-vis spectroscopy

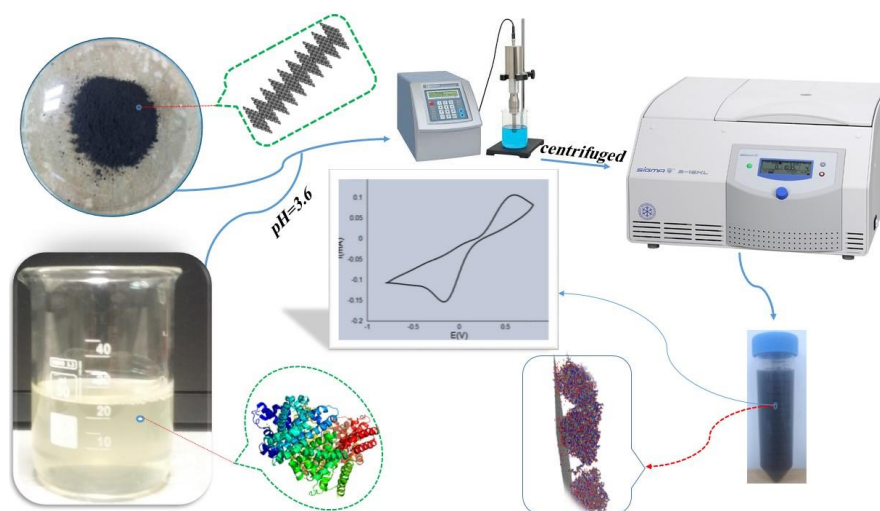


Figure 1. Graphical abstract of the G-BSA synthesized through sonication of graphite in presence of BSA.

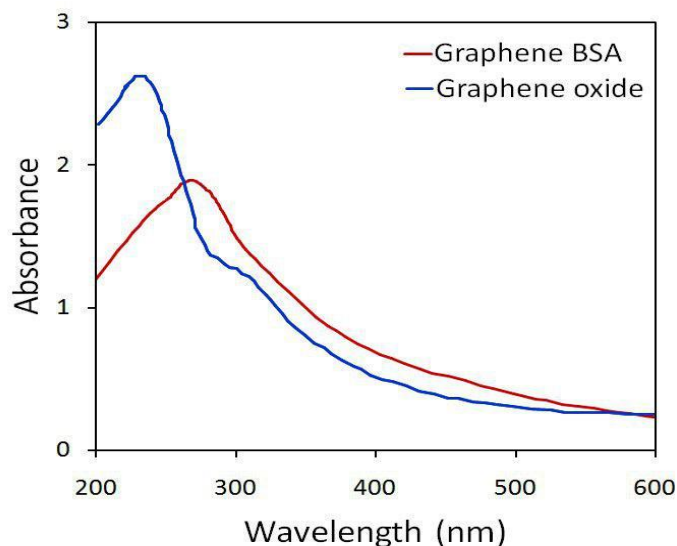
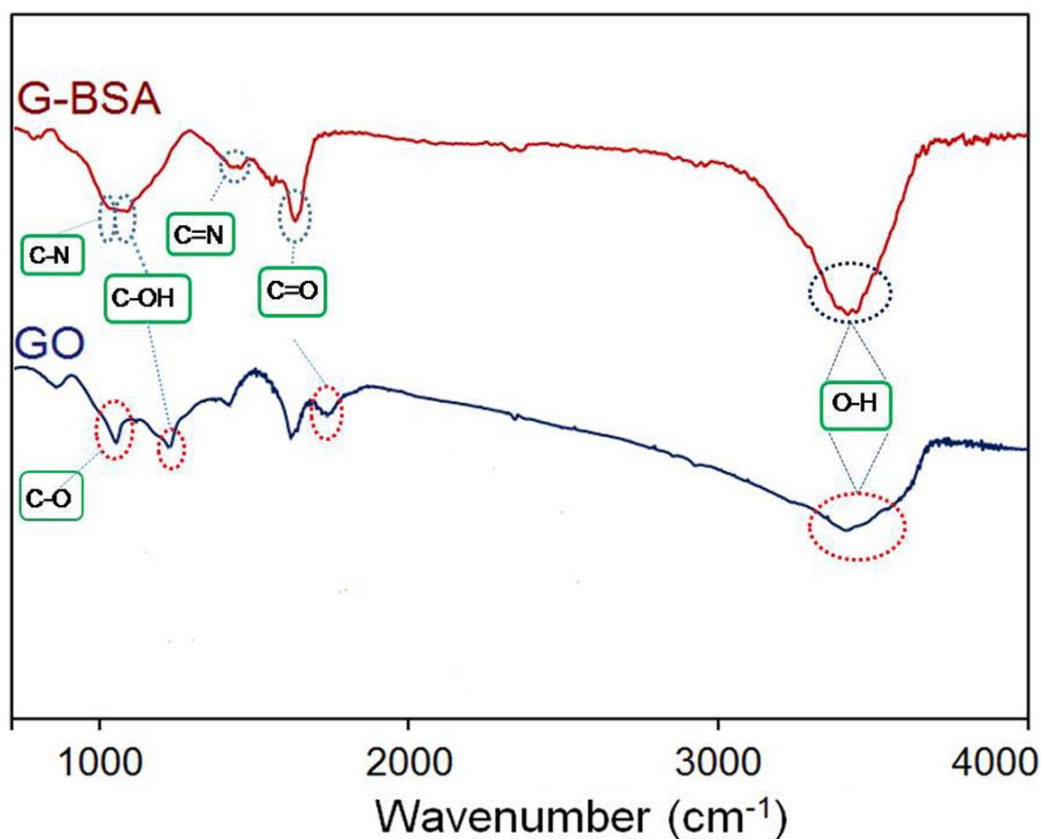


Figure 2. Uv-vis spectrums of G-BSA and GO. There are 2 peaks of 230 and 269 nm in the curves of the GO and G-BSA respectively, indicating that the synthesis of the GO and G-BSA were established successfully.

Synthesis of G-BSA and GO were first confirmed by uv-vis spectroscopy. In the Fig. 2, the synthesized G-BSA and GO exhibited a main peak in 269 and 230 nm. These observed peaks are the characteristics of graphene derivatives. It seems, functional groups in the G-BSA are responsible for the shift of G-BSA in uv-vis spectrum [22, 23].

### 3.2. FTIR spectrum

The peaks of 1098 and 1550  $\text{cm}^{-1}$ , in the FTIR spectrum of G-BSA, were observed in the Fig. 3; in which these peaks are attributed to stretching C-N and C=N (amine group), respectively [18]. The essence of these peaks corresponded to the reaction of tyrosine residues of BSA with graphene sheet. According to ionization of phenolic groups in BSA, these residues are capable to reduce and stabilize graphene sheets [24]. The 1720 and 1200  $\text{cm}^{-1}$  and 3430  $\text{cm}^{-1}$  wave numbers were related to the C=O and C-OH, O-H respectively. The peak at 1600  $\text{cm}^{-1}$  was ascribed to C=C aromatic vibration. The GO FTIR spectrum was shown in Fig. 3 [25]. Intense band at 1226  $\text{cm}^{-1}$  (C-OH stretching vibrations), 3430  $\text{cm}^{-1}$  (O-H stretching vibrations) and the bands at 1726  $\text{cm}^{-1}$  (C=O stretching vibrations from carbonyl and carboxylic groups) and 1103  $\text{cm}^{-1}$  (C-O stretching vibrations), are the most characteristic features of GO [26]. The comparison of the FTIR spectra of G-BSA and GO illustrated that the G-BSA possess amine groups and low O-H functional group that are essential and suitable for the biomedical application [26].



**Figure 3.** FTIR spectrum of G-BSA and GO.

### 3.3. AFM analysis

For measurement of the thickness of the samples, we utilized atomic force microscopy (AFM). In Fig.4, the height-profile images of G-BSA and GO sheets revealed that maximum thickness were in the range of 1-6.5 nm. These data indicated that the synthesized G-BSA sheets are single-layered to few-layered. Indeed, when BSA, a macromolecule, is attached to the graphene sheet, thickness of G-BSA is increased [19].

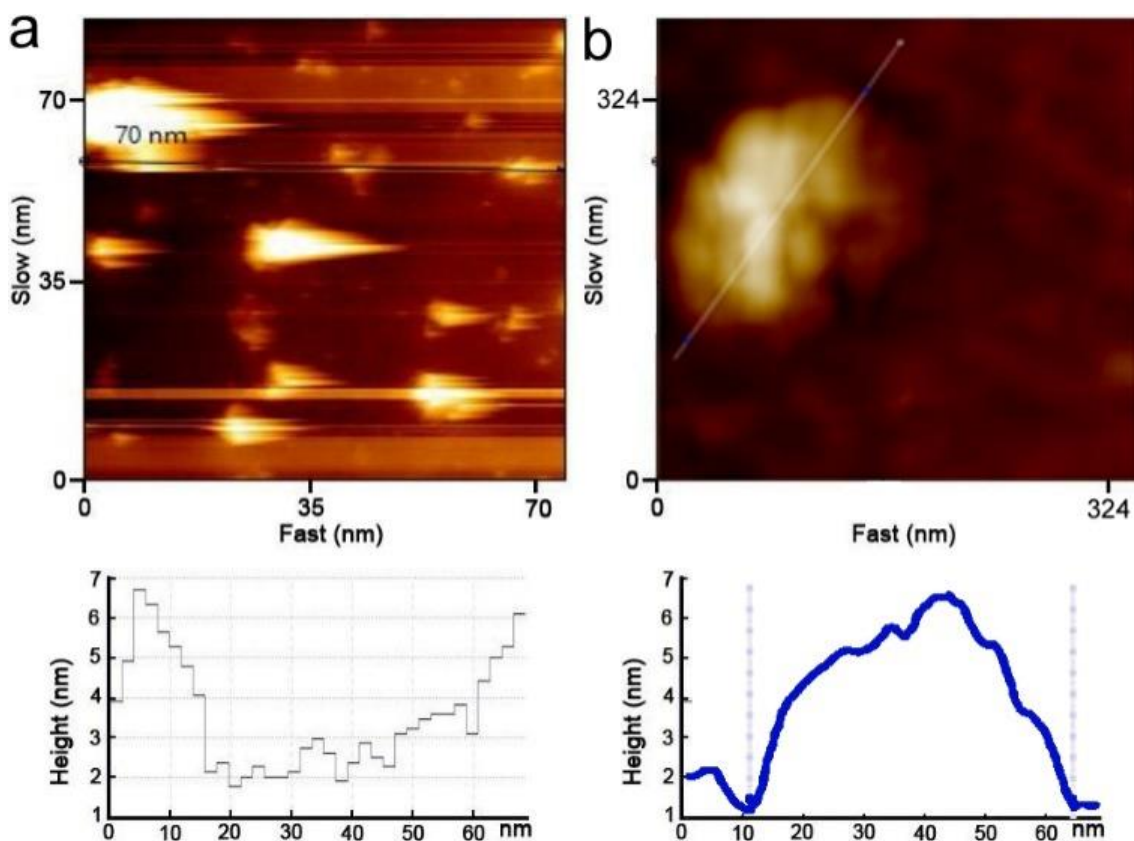


**Figure 4.** Atomic force microscopy (AFM) images and the cross –section graph of G-BSA and GO.

### 3.4. Raman spectroscopy

To evaluate the structure of graphene and confirm the AFM microscopy results, Raman spectroscopy was applied. In Fig. 5, the G, 2D and D bands located in  $1570$ ,  $2700$  and  $1350$   $\text{cm}^{-1}$  respectively, corresponded to the high quality graphene production [27]. In compare to the graphite, the appearing D band in Raman spectrum of G-BSA showed that the vibration was occurred in hexagonal carbon lattice [28, 29]. In other words, the  $\text{sp}^3$  hybridization was carried out with the functional groups that discussed in the FTIR part [30]. The ratio of D to G band intensities for the G-BSA was obtained 0.17. This ratio demonstrated that the  $\text{sp}^3$  hybridization was increased. In other words, attaching the functional groups was responsible for the increased  $\text{sp}^3$  hybridization [30]. For GO, D, G and 2D bands were related to  $1350$ ,  $1600$  and  $2750$   $\text{cm}^{-1}$  respectively.  $I_D/I_G$  for GO was obtained  $1/15$  which showed high oxidation degree of graphene [7].

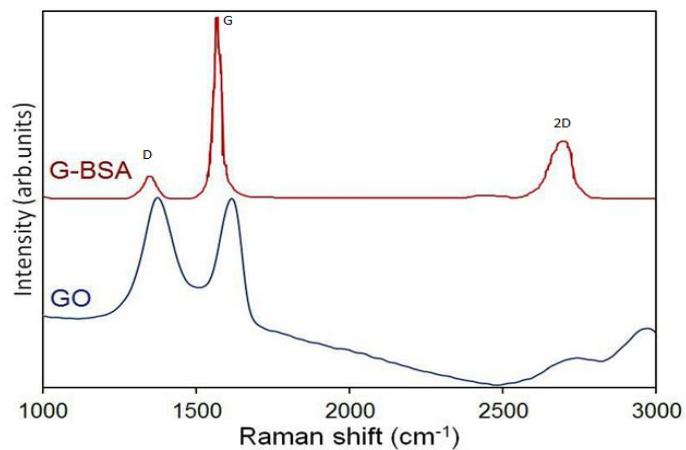


**Figure 5.** Raman spectrum of G-BSA and GO.

### 3.5. Scanning electron microscopy (SEM)

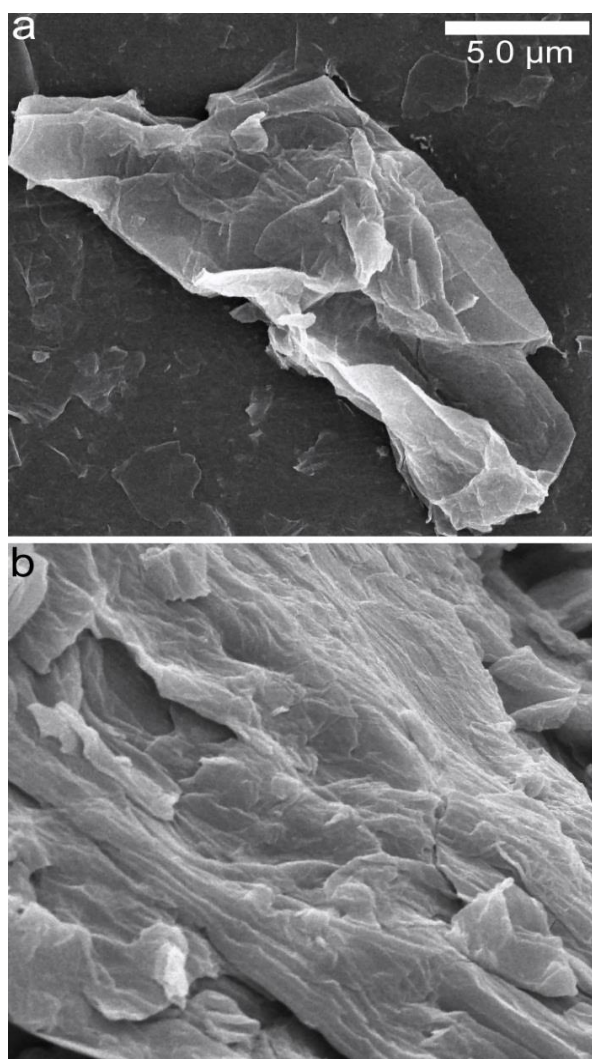


**Figure 6.** Field emission scanning electron microscopy (FESEM) images of G-BSA (a) and GO (b).

In Fig. 6, SEM images of G-BSA and GO were shown. These images were demonstrated that graphene sheet was a major content and negligible amount of graphite. The lateral dimension of graphene sheets was from tens nanometers to a few micrometers [31].

3.6. Electrochemical analysis

**Table 1.** Important electrochemical parameters extracted from the CVs and nyquist curves.

Working electrode	$J_{ox}$ (mA cm <sup>-2</sup> )	$R_{ct}$ (Ω)
FTO	0.08	11,000
GO	0.06	10000
G-BSA	0.11	8000

$J_{ox}$ ; oxidation current density.

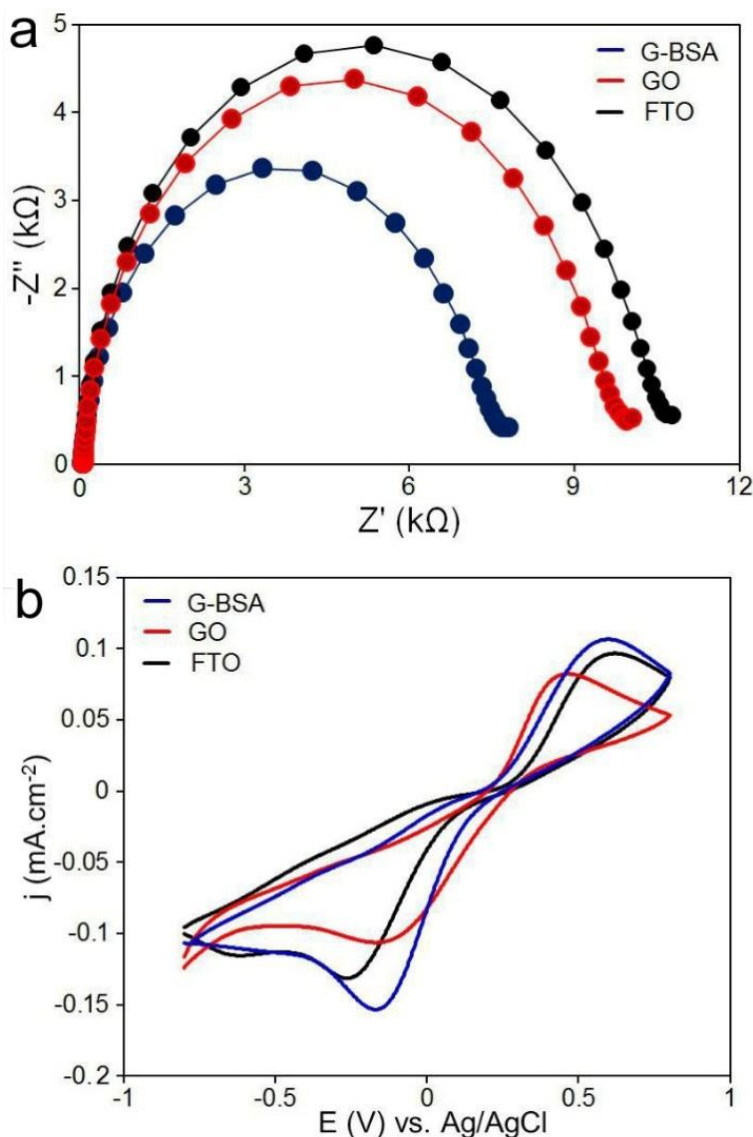


**Figure 7.** (a) Nyquist curves and (b) CVs for FTO electrode, GO and G-BSA. All measurements were established in 0.01 M PBS (pH 7.4) containing 5 mM  $K_3Fe(CN)_6$ .

Cyclic voltammograms (CVs) and nyquist curves were provided for the bare, GO and G-BSA electrodes (Fig. 7). Important parameters of the electrochemical characteristics of the electrodes were extracted from the Fig. 7 and summarized in the Table 1. According to the results, the critical modification of fluorine doped tin oxide (FTO) electrode with G-BSA improved the conductivity of the bare and GO-modified electrodes considerably and decreased the charge transfer resistance ( $R_{ct}$ ). This phenomena was verified in the literature already [32]. In upper curves (Nyquist plot), the semicircle portion was observed at high frequencies corresponded to  $R_{ct}$  that could be evaluated directly as the semicircle diameter. A linear part was predicted in the Nyquist plot at low frequencies due to the limited mass transfer that could be concluded with G-BSA modified electrode [33]. Increasing the conductivity, upon arrival of  $Fe(CN)_6^{3-}$  probe to the electrode surface electron transfer occurred with high speed due to the formation of diffusion layer and the limitation of mass transfer. According to Fig. 7, there is suitable conformity between CVs and Nyquist curves as with decreasing the  $R_{ct}$ , the peak height in CV was enhanced. The maximum charge transfers resistance ( $R_{ct}$ ) was  $\sim 11,000 \Omega$  for bare FTO and at lowest (the best) was  $\sim 8000 \Omega$  for the G-BSA modified electrode.

### 3.7. Ascorbic acid determination

Ascorbic acid (AA) is an essential element in synthesis and maintenance of the protein collagen in tissue regeneration [34]. Therefore, AA was tested on the G-BSA modified electrode to assess its performance. Calibration curves extracted from amperometry technique represented a linear range for the G-BSA modified electrode (Fig. 8). The linear sensing range was achieved for the sensor. The analyte detection limit ( $S/N = 3$ ) and the linear sensing range of the optimized biosensor was compared to AA sensors comprising the similar materials (Table 2). The linear sensing range of the developed biosensor was wider than some other nanostructured biosensors reported in the literature (Table 2). The current response of the GO-modified electrode was negligible and poor. It seems that the BSA with a lot of amino acids and protein catalytic activity could be established these desirable results.

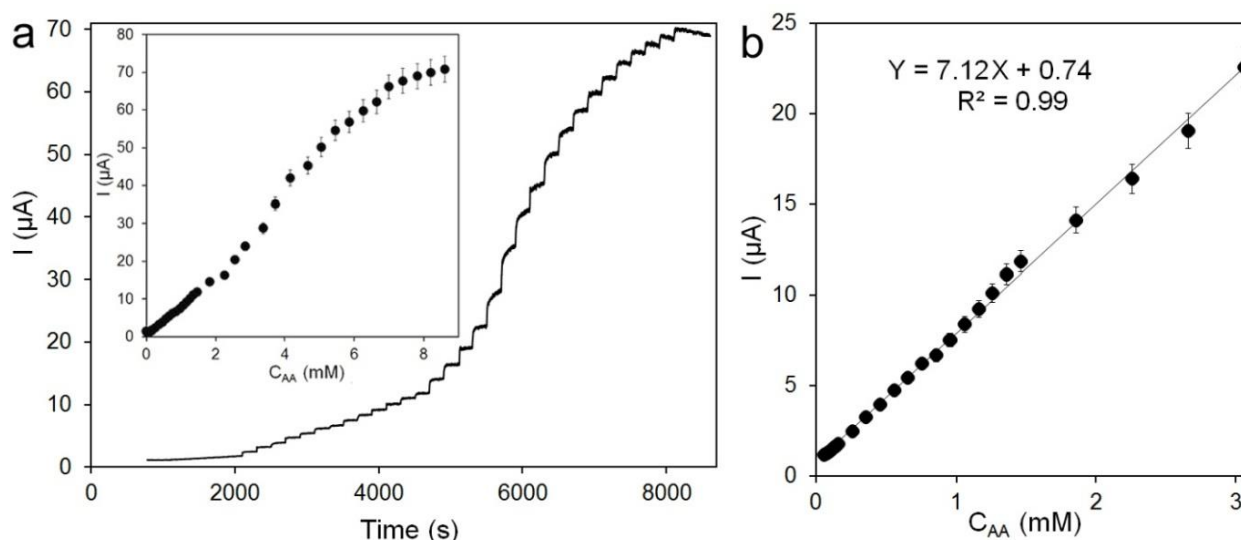


**Figure 8.** (a) and (b) represent amperometric responses and linear range, respectively. Inset illustrates the calibration curve (linear range) of the sensor to oxidation of AA.

**Table 2.** The comparison of the sensor responses of the present work with other studies in the literature.

Electrode materials	Detection limit ( $\mu\text{M}$ )	Linear range ( $\mu\text{M}$ )	Reference
PANI/PSS/Gr	5	100-1000	[35]
NG	2.2	5-1300	[36]
CoPc-MWCNTs	1	10-2600	[37]
AGCE/ASOD	2	5-400	[38]
PdNi/C nanomaterials	0.5	10-1800	[39]
MWCNT/CCE	7.71	15-800	[40]
Pt-Au hybrid	103	103-165	[41]
Chitosan-graphene	50	50-1200	[42]
OMC/Nafion	20	40-800	[43]
ZnO/RM	1.4	15-240	[44]
MBMOR/P	12.1	20-800	[45]
Pd/CNFs	15	50-4000	[46]
PMPy/Pd-nanoclusters	1000	50-1000	[47]
DB71	1	1-2000	[48]
BPPF <sub>6</sub> /CPE	8	10-3000	[49]
PPF/GNS	120	400-6000	[50]
PdNPs-GO	-	20-2280	[51]
Pt/Au/GCE	-	24-384	[41]
G-BSA	25	50-3000	<b>Present work</b>

When bovine serum albumin (BSA), a protein with isoelectric point at 4.5 pH, that possess hydrophobic and hydrophilic amino acids, was ultrasounded, the layer exfoliation was beginning. The role of BSA in the graphite solution was stabilizing the synthesized graphene sheets. Hydrophobic amino acids reacted with the carbon in the plan and edge of graphene sheets. The hydrophilic amino acids of BSA was responsible to make an aqueous dispersion of graphene.

The power of ultrasonic is a critical key needed to be adjusted. Synthesis of graphene through this method could be a suitable approach for future biomedical applications. Other proteins could be used to graphene production but should be checked in terms of energetically and structurally.

#### 4. CONCLUSION

In summary, a low cost and green approach to synthesis of graphene was reported and named G-BSA in the progress of paper. The graphene was characterized by the spectroscopic techniques such as uv-vis, FTIR and Raman spectroscopy. AFM was used for evaluating the thickness of graphene layer and SEM and TEM results were shown the lateral dimension of graphene sheets. After synthesis process, G-BSA was applied to investigate the electrochemical and biosensing properties. We utilized G-BSA in electrochemical field as an application that showed amazing results, but it is still capable to use in drug delivery, imaging, biosensors and other biomedical applications.

## References

1. O. M. Koo, I. Rubinstein and H. Onyuksel, *Nanomedicine-UK*, 1 (2005) 193.
2. A. K. Geim and K.S. Novoselov, *Nat. Mater.*, 6 (2007) 183.
3. K. S. Novoselov, A.K. Geim, S. Morozov, D. Jiang, M. Katsnelson, I. Grigorieva, S. Dubonos and Firsov, AA, *Nature*, (2005) 1.
4. X. Cui, C. Zhang, R. Hao and Y. Hou, *Nanoscale*, 3 (2011) 2118.
5. S. Alwarappan, A. Erdem, C. Liu and C.-Z. Li, *J. Phys. Chem. C.*, 113 (2009) 8853.
6. T. J. Davies, M. E. Hyde and R. G. Compton, *Angew. Chem-Ger. Edit.*, 117 (2005) 5251.
7. V. Georgakilas, J.N. Tiwari, K.C. Kemp, J.A. Perman, A.B. Bourlinos, K.S. Kim and R. Zboril, *Chem. Rev.*, 116 (2016) 5464.
8. R. Li, X. Dong, C. He, Z. Liu, L. Huang and Y. Yang, *Int. J. Electrochem. Sci.*, 12 (2017) 144.
9. Y. Wang, Y. Shao, D. W. Matson and J. Li, Y. Lin, *ACS. Nano.*, 4 (2010) 1790.
10. D. Boukhalov and M. Katsnelson, *Nano. lett.*, 8 (2008) 4373.
11. S. U. Lee, R. V. Belosludov, H. Mizuseki and Y. Kawazoe, *Small*, 5 (2009) 1769.
12. R. S. Sundaram, C. Gómez-Navarro, K. Balasubramanian, M. Burghard and K. Kern, *Adv. Mater.*, 20 (2008) 3050.
13. M. H. Mustafa and A. Zdunek, *Int. J. Electrochem. Sci.*, 12 (2017) 2917.
14. P. Sharma, S. K. Tuteja, V. Bhalla, G. Shekhawat, V. P. Dravid and C. R. Suri, *Biosens. Bioelectron.*, 39 (2013) 99.
15. C. Shan, H. Yang, J. Song, D. Han, A. Ivaska and L. Niu, *Anal. Chem.*, 81 (2009) 2378.
16. Z. Tang, H. Wu, J. R. Cort, G. W. Buchko, Y. Zhang, Y. Shao, I. A. Aksay, J. Liu and Y. Lin, *Small*, 6 (2010) 1205.
17. W. Hong, H. Bai, Y. Xu, Z. Yao, Z. Gu and G. Shi, *J. Phys. Chem. C*, 114 (2010) 1822.
18. J. Liu, S. Fu, B. Yuan, Y. Li and Z. Deng, *J. Am. Chem. Soc.*, 132 (2010) 7279.
19. S. Ahadian, M. Estili, V. J. Surya, J. Ramón-Azcón, X. Liang, H. Shiku, M. Ramalingam, T. Matsue, Y. Sakka and H. Bae, *Nanoscale*, 7 (2015) 6436.
20. H. Yu, B. Zhang, C. Bulin, R. Li and R. Xing, *Sci. Rep-UK.*, 6 (2016) 36143.
21. J. Chen, B. Yao, C. Li and G. Shi, *Carbon.*, 64 (2013) 225.
22. D. Li, M.B. Müller, S. Gilje, R.B. Kaner and G.G. Wallace, *Nat. Nanotechnol.*, 3 (2008) 101.
23. B. Schwenzler, T. C. Kaspar, Y. Shin and D. W. Gotthold, *J. Phys. Chem. C.*, 120 (2016) 12559.
24. P. Selvakannan, A. Swami, D. Srisathiyarayanan, P. S. Shirude, R. Pasricha, A.B. Mandale and M. Sastry, *Langmuir*, 20 (2004) 7825.
25. S. Chaiyakun, N. Witit-Anun, N. Nuntawong, P. Chindaudom, S. Oaew, C. Kedkeaw and P. Limsuwan, *Procedia. Engineer.*, 32 (2012) 759.
26. S. Das, S. Singh, V. Singh, D. Joung, J. M. Dowding, D. Reid, J. Anderson, L. Zhai, S.I. Khondaker and W.T. Self, *Part. Part. Syst. Char.*, 30 (2013) 148.
27. L. Malard, M. Pimenta, G. Dresselhaus and M. Dresselhaus, *Phys. Rep.*, 473 (2009) 51.
28. A.C. Ferrari, *Solid state communications*, 143 (2007) 47.
29. M. Wall, The Raman spectroscopy of graphene and the determination of layer thickness, WI Thermo Fisher Scientific <http://www.thermoscientific.com/content>, (2011) Madison, United states.
30. R. Beams, L. G. Cançado and L. Novotny, *J. Phys.*, 27 (2015) 083002.
31. S. Stankovich, D. A. Dikin, R. D. Piner, K. A. Kohlhaas, A. Kleinhammes, Y. Jia, Y. Wu, S.T. Nguyen and R.S. Ruoff, *Carbon*, 45 (2007) 1558.
32. A. Rose, N. Raghavan, S. Thangavel, B. U. Maheswari, D. P. Nair and G. Venugopal, *Mat. Sci. Semicon. Proc.*, 31 (2015) 281.
33. J. Yang and S. Gunasekaran, *Carbon*, 51 (2013) 36.
34. P. Janda, J. Weber, L. Dunsch and A. Lever, *Anal. Chem.*, 68 (1996) 960.
35. J. Luo, S. Jiang, R. Liu, Y. Zhang and X. Liu, *Electrochim. Acta*, 96 (2013) 103.

36. Z. H. Sheng, X. Q. Zheng, J. Y. Xu, W. J. Bao, F. B. Wang and X. H. Xia, *Biosens. Bioelectron.*, 34 (2012) 125.
37. X. Zuo, H. Zhang and N. Li, *Sens. Actuat. B.*, 161 (2012) 1074.
38. X. Wang, H. Watanabe and S. Uchiyama, *Talanta*, 74 (2008) 1681.
39. X. Zhang, Y. Cao, S. Yu, F. Yang and P. Xi, *Biosens. Bioelectron.*, 44 (2013) 183.
40. B. Habibi and M. H. Pournaghi-Azar, *Electrochim. Acta*, 55 (2010) 5492.
41. S. Thiagarajan and S. M. Chen, *Talanta*, 74 (2007) 212.
42. D. Han, T. Han, C. Shan, A. Ivaska and L. Niu, *Electroanal.*, 22 (2010) 2001.
43. D. Zheng, J. Ye, L. Zhou, Y. Zhang and C. Yu, *J. Electroanal. Chem.*, 625 (2009) 82.
44. C. F. Tang, S. A. Kumar and S. M. Chen, *Anal. Biochem.*, 380 (2008) 174-183.
45. M. Arvand, S. Sohrabnezhad, M. Mousavi, M. Shamsipur and M. Zanjanchi, *Anal. Chim. Acta*, 491 (2003) 193.
46. J. Huang, Y. Liu, H. Hou and T. You, *Biosens. Bioelectron.*, 24 (2008) 632.
47. N. F. Atta, M. F. El-Kady and A. Galal, *Anal. Biochem.*, 400 (2010) 78.
48. S. A. Kumar, P. H. Lo and S. M. Chen, *Biosens. Bioelectron.*, 24 (2008) 518.
49. W. Sun, M. Yang, R. Gao and K. Jiao, *Electroanal.*, 19 (2007) 1597.
50. G. P. Keeley, A. O'Neill, N. McEvoy, N. Peltekis, J. N. Coleman and G. S. Duesberg, *J. Mater. Chem.*, 20 (2010) 7864.
51. G. H. Wu, Y. F. Wu, X. W. Liu, M. C. Rong, X. M. Chen and X. Chen, *Anal. Chim. Acta*, 745 (2012) 33.

© 2018 The Authors. Published by ESG ([www.electrochemsci.org](http://www.electrochemsci.org)). This article is an open access article distributed under the terms and conditions of the Creative Commons Attribution license (<http://creativecommons.org/licenses/by/4.0/>).